Hindawi
Mathematical Problems in Engineering
Volume 2022, Article ID 7880806, 15 pages
https://doi.org/10.1155/2022/7880806

Research Article

Time Period Analysis of Orthotropic Skew Plate with 2-D Circular Thickness and 1-D Circular Density

Neeraj Lather, Reeta Bhardwaj, Amit Sharma, and Kamal Kumar

Department of Mathematics, Amity School of Applied Sciences, Amity University Haryana, Gurugram, India

Correspondence should be addressed to Amit Sharma; dba.amitsharma@gmail.com and Kamal Kumar; kamalkumarrajput92@gmail.com

Received 4 August 2022; Revised 9 September 2022; Accepted 24 September 2022; Published 17 October 2022

Academic Editor: Alessandro Lo Schiavo

In the present study, the time period of vibration of an orthotropic parallelogram plate with 2–D (two-dimensional) circular thickness under the effect of 2–D parabolic temperature is investigated for the first time. The different edge conditions are *CCCC*, *CCCF*, *CFCF*, *CSCF*, and *SFSF* boundary conditions, where C, S, and F stands for clamped, simply supported, and free edges of the plate, respectively. The variation in density of plate material is considered to be 1–D (one-dimensional) circular. The Rayleigh–Ritz technique is used to solve the differential equation and evaluate the time period for the first two modes of vibration. A convergence study of an orthotropic parallelogram, rectangle plate, and square plate for modes of frequency at various edge conditions is also carried out. The authors performed a comparative analysis of the time period and modes of frequency of orthotropic parallelogram, rectangle plate, and isotropic square plate with the available published results at various edge conditions. The main conclusion which we made from this study is that by choosing the above-mentioned plate parameters, we obtained fewer modes of frequency in comparison to other variations mentioned in the literature. Also, the study suggests that the variation in modes of frequency is less in comparison to other variations.

1. Introduction

In engineering, machines and structures vibrate, so we cannot proceed without considering vibration. Modern technology requires knowing the vibration characteristics of plates with different plate parameters. Tapered plates with uniform and nonuniform thickness under a temperature environment are generally utilized in the aeronautical field, construction industry, and submarine structures. Different analysts/researchers investigated the vibration characteristics of various plates (homogeneous or nonhomogeneous) having variable thickness with or without consideration of temperature effect. A significant work about the vibrational characteristics of plates has been reported in the literature.

The quasi-green function method (QGFM) [1] is applied to solve the free vibration of clamped orthotropic thin plates (parallelogram shape) on the Winkler foundation. In this study, a quasi-green function is established by using the fundamental solution and a principal differential equation has been solved with the help of the variable separable method. Vibration of the viscoelastic orthotropic parallelogram plate with parabolic [2] and linear thickness [3] at clamped boundary conditions was studied by using the Rayleigh–Ritz technique to determine the frequency equation. The frequency equation is derived by using the Rayleigh–Ritz technique, and two-term deflection function is used to find the modes of frequency for various values of taper constants, aspect ratios, and skew angle. Rayleigh–Ritz technique is employed to study the natural vibration of the nonhomogeneous tapered parallelogram plate with two-dimensional varying thickness [4] and one-dimensional circular variation in density parameter [5] at clamped boundary conditions under temperature field. The time period of natural transverse vibration of a nonhomogeneous skew (parallelogram) plate [6] with variable thickness and temperature field has been investigated on clamped and combination of clamped and simply supported edge conditions. The effect of sinusoidal varying thickness [7] on the vibrations of nonhomogeneous parallelogram plates is computed at clamped edges. Here, the frequency equation is solved by using the Rayleigh–Ritz method and we analyze the vibrational behavior of frequencies of a parallelogram plate for both modes. The effect of two-dimensional circular variations in thickness [8] on a nonhomogeneous parallelogram plate under thermal effect was computed, and differential equations of motions are solved by using the Rayleigh–Ritz technique and we evaluate the vibrational frequencies at various plate parameters. A fast-converging semianalytical method [9] was developed for assessing the vibration effect on thin orthotropic skew plates. An experimental and finite element [10] was proposed to study the free vibration of isotropic and laminated composite skew plates. A method to unify the solutions for plates with different shapes [11] (circular plate, annular plate, circular sector plate, and annular sector plate) subjected to general boundary conditions was adapted to study vibration characteristics. The time period of a rectangular plate [12] with variable thickness and temperature effect was analyzed. Two-dimensional circular thickness effects on time period of the nonhomogeneous skew plate [13] for variable temperature environments are computed at various combinations of clamped, simply supported, and free edge conditions. Free vibration of an orthotropic parallelogram plate [14] with a simply supported boundary condition under the effect of biparabolic thickness variation and linear temperature distribution in both directions is carried out at simply supported edges. The effect of parabolically thick variation on vibration of a viscoelastic orthotropic parallelogram plate [15] having clamped boundary conditions on all four edges was studied by using the separation of variables method. Vibration and modes of nanocomposite plates, functionally graded sandwich plates, sector plates, sandwich panels, l-shaped graphene sheet, skew plate, cylindrical skew plates, functionally graded rectangle plates, spherical shell, and annular sector plates [16–37] have been analyzed.

In the literature till date, researchers have studied the 1–D (one-dimensional) circular tapering impact on vibrational modes of frequency for different isotropic plate structures. But in the case of orthotropic material, none of the researchers have tackled 1–D (one-dimensional) circular tapering as well as 2–D (two-dimensional) circular tapering impact on the mode of frequency. In this work, we aim to fill up this research gap. Also, none of the researchers have aimed to tackle the 2–D circular tapering impact on the mode of frequency in the case of orthotropic parallelogram plate. We will also address this issue.

In this paper, the authors studied the impact of 2–D (two-dimensional) circular tapering on the time period of vibrational modes of frequency of the nonhomogeneous orthotropic parallelogram plate on *CCCC*, *CCCF*, *CFCF*, *CSCF*, and *SFSF* boundary conditions. The authors also evaluated 1–D (one-dimensional) circular density and 2–D (two-dimensional) parabolic temperature impacts on the time period of vibrational modes of frequency. All the results displayed in the tabular form (refer Tables 1–3). In order to authenticate our findings, authors performed comparatively analysis of time period and modes of frequency of the orthotropic parallelogram plate (*SSSS* and *CCCC* edge condition), rectangle plate (*CCCC* edge condition), and square plate (*CCCC*, *SCSC*, *FCFC*, and *FSFS* edge conditions) with the available published results (refer Tables4–10).

2. Analysis

The orthotropic parallelogram plates made with nonhomogeneous material properties with variable thickness l having skew angle θ, length a, breadth b, density ρ, and Poisson's ratio ν referred to the skew coordinates $\zeta = x - y\tan\theta$ and $\psi = y\sec\theta$ (refer Figure 1).

The thickness l of the skew plate is assumed to be circular in both dimensions (refer Figure 2), and density ρ is assumed to circular in one dimension as

$$l = l_0\left[1+\beta_1\left(1-\sqrt{1-\frac{\zeta^2}{a^2}}\right)\right]\left[1+\beta_2\left(1-\sqrt{1-\frac{\psi^2}{b^2}}\right)\right],$$
$$\rho = \rho_0\left[1-m\left(1-\sqrt{1-\frac{\zeta^2}{a^2}}\right)\right], \tag{1}$$

where l_0 and ρ_0 are the thickness and density of the plate, respectively, at the origin. Also, $\beta_1, \beta_2\,(0 \le \beta_1, \beta_2 \le 1)$ and $m\,(0 \le m < 1)$ are taper parameters and nonhomogeneity parameter, respectively.

Two-dimensional steady state temperature variations on the plate are considered to be parabolic as taken in [13]

$$\tau = \tau_0\left(1-\frac{\zeta^2}{a^2}\right)\left(1-\frac{\psi^2}{b^2}\right), \tag{2}$$

where τ and τ_0 denotes the temperature excess above the reference temperature on the plate at any point and at the origin, respectively.

The temperature-dependent modulus of elasticity for engineering structures is taken as in [14]

$$E_\zeta(\tau) = E_1(1-\gamma\tau),\ E_\psi(\tau) = E_2(1-\gamma\tau),$$
$$G_{\zeta\psi}(\tau) = G_0(1-\gamma\tau), \tag{3}$$

where E_ζ and E_ψ are Young's moduli in ζ and ψ directions, respectively, $G_{\zeta\psi}$ is shear modulus, and γ is taken as the slope variation of moduli with temperature.

Substituting (2) in (3), we get the following expressions:

$$E_\zeta(\tau) = E_1\left[1-\alpha\left(1-\frac{\zeta^2}{a^2}\right)\left(1-\frac{\psi^2}{b^2}\right)\right],$$
$$E_\psi(\tau) = E_2\left[1-\alpha\left(1-\frac{\zeta^2}{a^2}\right)\left(1-\frac{\psi^2}{b^2}\right)\right], \tag{4}$$
$$G_{\zeta\psi}(\tau) = G_0\left[1-\alpha\left(1-\frac{\zeta^2}{a^2}\right)\left(1-\frac{\psi^2}{b^2}\right)\right],$$

where $\alpha = \gamma\tau_0$, $(0 \le \alpha < 1)$ is called the temperature gradient.

Table 1: Time period of the orthotropic parallelogram plate at *CCCC*, *CCCF*, *CFCF*, *CSCF*, and *SFSF* edge conditions corresponding to both tapering parameters β_1 and β_2.

		$m = 0.2$, $\alpha = 0.4$											
	β_1	$\beta_2 = 0.0$		$\beta_2 = 0.2$		$\beta_2 = 0.4$		$\beta_2 = 0.6$		$\beta_2 = 0.8$		$\beta_2 = 1.0$	
		K_1	K_2	K_1	K_2	K_1	K_2	K_1	K_2	K_1	K_2	K_1	K_2
CCCC	0.0	0.16309	0.62562	0.15807	0.60548	0.15315	0.58591	0.14831	0.56693	0.14362	0.54865	0.13905	0.53102
	0.2	0.15367	0.59097	0.14909	0.57262	0.14457	0.55471	0.14013	0.53734	0.13581	0.52059	0.13160	0.50445
	0.4	0.14441	0.55792	0.14022	0.54114	0.13608	0.52474	0.13201	0.50884	0.12803	0.49345	0.12416	0.47862
	0.6	0.13551	0.52688	0.13167	0.51155	0.12788	0.49650	0.12415	0.48192	0.12049	0.46778	0.11692	0.45412
	0.8	0.12710	0.49816	0.12358	0.48403	0.12010	0.47020	0.11667	0.45676	0.11330	0.44372	0.11001	0.43109
	1.0	0.11926	0.47168	0.11603	0.45864	0.11282	0.44586	0.10965	0.43345	0.10654	0.42135	0.10351	0.40966
CCCF	0.0	0.18375	0.59876	.17094	0.56505	0.15918	0.53461	0.14848	0.50709	0.13883	0.48205	0.13011	0.45921
	0.2	0.17587	0.56935	0.16385	0.53834	0.15277	0.51026	0.14266	0.48465	0.13350	0.46128	0.12522	0.43992
	0.4	0.16788	0.54054	0.15665	0.51218	0.14625	0.48629	0.13673	0.46254	0.12808	0.44083	0.12024	0.42085
	0.6	0.15993	0.51293	0.14948	0.48695	0.13976	0.46310	0.13082	0.44114	0.12267	0.42094	0.11527	0.40228
	0.8	0.15215	0.48676	0.14245	0.46295	0.13338	0.44095	0.12501	0.42063	0.11735	0.40181	0.11036	0.38441
	1.0	0.14465	0.46219	0.13564	0.44033	0.12719	0.42000	0.11936	0.40115	0.11216	0.38365	0.10559	0.36741
CFCF	0.0	0.36163	0.78754	0.34906	0.74915	0.33628	0.71107	0.32349	0.67419	0.31091	0.63900	0.29866	0.60589
	0.2	0.34291	0.72835	0.33134	0.69379	0.31947	0.65955	0.30755	0.62625	0.29574	0.59442	0.28419	0.56439
	0.4	0.32421	0.67356	0.31352	0.64252	0.30249	0.61164	0.29132	0.58157	0.28022	0.55286	0.26933	0.52565
	0.6	0.30590	0.62420	0.29599	0.59612	0.28567	0.56819	0.27519	0.54111	0.26474	0.51507	0.25444	0.49040
	0.8	0.28826	0.58016	0.27902	0.55474	0.26934	0.52945	0.25948	0.50489	0.24959	0.48129	0.23985	0.45892
	1.0	0.27148	0.54123	0.26282	0.51811	0.25372	0.49512	0.24440	0.47275	0.23504	0.45129	0.22581	0.43090
CSCF	0.0	0.37061	0.76699	0.35126	0.70598	0.33276	0.65188	0.31529	0.60416	0.29896	0.56194	0.28379	0.52462
	0.2	0.35541	0.70202	0.33697	0.64698	0.31925	0.59800	0.30253	0.55471	0.28689	0.51638	0.27234	0.48242
	0.4	0.33964	0.64252	0.32201	0.59291	0.30508	0.54871	0.28907	0.50950	0.27409	0.47473	0.26014	0.44391
	0.6	0.32358	0.58971	0.30674	0.54491	0.29051	0.50501	0.27515	0.46948	0.26079	0.43800	0.24743	0.41001
	0.8	0.30755	0.54353	0.29139	0.50310	0.27581	0.46694	0.26106	0.43480	0.24726	0.40621	0.23445	0.38070
	1.0	0.29174	0.50354	0.27620	0.46694	0.26121	0.43417	0.24703	0.40492	0.23379	0.37888	0.22149	0.35560
SFSF	0.0	0.29229	1.6282	0.28379	1.5506	0.27512	1.4737	0.26640	1.3990	0.25774	1.3275	0.24924	1.2597
	0.2	0.27132	1.5574	0.26415	1.4821	0.25676	1.4077	0.24927	1.3356	0.24179	1.2666	0.23439	1.2013
	0.4	0.25116	1.4899	0.24510	1.4165	0.23879	1.3442	0.23236	1.2744	0.22589	1.2078	0.21944	1.1449
	0.6	0.23233	1.4263	0.22716	1.3545	0.22175	1.2840	0.21619	1.2162	0.21056	1.1517	0.20492	1.0910
	0.8	0.21506	1.3666	0.21059	1.2962	0.20590	1.2274	0.20106	1.1614	0.19612	1.0989	0.19117	1.0401
	1.0	0.19938	1.3107	0.19549	1.2416	0.19137	1.1744	0.18711	1.1101	0.18275	1.0493	0.17836	0.99243

Table 2: Time period of the orthotropic parallelogram plate at *CCCC*, *CCCF*, *CFCF*, *CSCF*, and *SFSF* edge conditions corresponding to thermal gradient α.

		$m = 0.2$											
	α	$\beta_1 = \beta_2 = 0.0$		$\beta_1 = \beta_2 = 0.2$		$\beta_1 = \beta_2 = 0.4$		$\beta_1 = \beta_2 = 0.6$		$\beta_1 = \beta_2 = 0.8$		$\beta_1 = \beta_2 = 1.0$	
		K_1	K_2	K_1	K_2	K_1	K_2	K_1	K_2	K_1	K_2	K_1	K_2
CCCC	0.0	0.14745	0.56414	0.13598	0.51987	0.12512	0.47909	0.11500	0.44190	0.10566	0.40825	0.09710	0.37800
	0.2	0.15468	0.59241	0.14208	0.54428	0.13026	0.50027	0.11931	0.46046	0.10928	0.42474	0.10015	0.39276
	0.4	0.16309	0.62562	0.14909	0.57262	0.13608	0.52474	0.12415	0.48192	0.11330	0.44372	0.10351	0.40966
	0.6	0.17303	0.66527	0.15724	0.60627	0.14275	0.55368	0.12961	0.50712	0.11779	0.46593	0.10722	0.42949
	0.8	0.18503	0.71396	0.16688	0.64711	0.15050	0.58858	0.13586	0.53740	0.12286	0.49257	0.11135	0.45311
CCCF	0.0	0.17190	0.55465	0.15450	0.50036	0.13884	0.45314	0.12490	0.41196	0.11258	0.37596	0.10171	0.34432
	0.2	0.17753	0.57532	0.15898	0.51821	0.14241	0.46870	0.12776	0.42569	0.11489	0.38814	0.10360	0.35519
	0.4	0.18375	0.59876	0.16385	0.53834	0.14625	0.48629	0.13082	0.44114	0.11735	0.40181	0.10559	0.36741
	0.6	0.19066	0.62574	0.16920	0.56150	0.15043	0.50633	0.13411	0.45874	0.11997	0.41736	0.10770	0.38117
	0.8	0.19839	0.65747	0.17508	0.58855	0.15496	0.52971	0.13764	0.47909	0.12275	0.43517	0.10993	0.39694
CFCF	0.0	0.32761	0.72420	0.30262	0.64629	0.27855	0.57498	0.25551	0.51170	0.23363	0.45676	0.21303	0.40960
	0.2	0.34338	0.75380	0.31601	0.66866	0.28980	0.59219	0.26484	0.52553	0.24126	0.46826	0.21918	0.41959
	0.4	0.36163	0.78754	0.33134	0.69379	0.30249	0.61164	0.27519	0.54111	0.24959	0.48129	0.22581	0.43090
	0.6	0.38312	0.82668	0.34906	0.72263	0.31689	0.63372	0.28676	0.55886	0.25875	0.49628	0.23298	0.44388
	0.8	0.40888	0.87292	0.36986	0.75625	0.33348	0.65948	0.29977	0.57963	0.26885	0.51375	0.24073	0.45918

Table 2: Continued.

	α	$m = 0.2$											
		$\beta_1 = \beta_2 = 0.0$		$\beta_1 = \beta_2 = 0.2$		$\beta_1 = \beta_2 = 0.4$		$\beta_1 = \beta_2 = 0.6$		$\beta_1 = \beta_2 = 0.8$		$\beta_1 = \beta_2 = 1.0$	
		K_1	K_2	K_1	K_2	K_1	K_2	K_1	K_2	K_1	K_2	K_1	K_2
CSCF	0.0	0.34199	0.73689	0.31288	0.62662	0.28512	0.53401	0.25890	0.45792	0.23429	0.39622	0.21136	0.34639
	0.2	0.35544	0.75147	0.32424	0.63649	0.29461	0.54111	0.26668	0.46351	0.24055	0.40096	0.21629	0.35073
	0.4	0.37061	0.76699	0.33697	0.64698	0.30508	0.54871	0.27515	0.46948	0.24726	0.40621	0.22149	0.35560
	0.6	0.38789	0.78358	0.35123	0.65817	0.31670	0.55688	0.28443	0.47611	0.25449	0.41205	0.22699	0.36110
	0.8	0.40784	0.80142	0.36747	0.67017	0.32971	0.56574	0.29460	0.48343	0.26225	0.41865	0.23277	0.36735
SFSF	0.0	0.26839	1.4686	0.24490	1.3499	0.22325	1.2354	0.20355	1.1270	0.18578	1.0257	0.16983	0.93243
	0.2	0.27958	1.5420	0.25398	1.4111	0.23062	1.2862	0.20959	1.1689	0.19075	1.0602	0.17394	0.96089
	0.4	0.29229	1.6282	0.26415	1.4821	0.23879	1.3442	0.21619	1.2162	0.19612	1.0989	0.17836	0.99243
	0.6	0.30692	1.7316	0.27564	1.5656	0.24788	1.4115	0.22345	1.2703	0.20198	1.1424	0.18314	1.0276
	0.8	0.32396	1.8591	0.28876	1.6665	0.25810	1.4910	0.23149	1.3331	0.20839	1.1921	0.18832	1.0671

Table 3: Time period of the orthotropic parallelogram plate at *CCCC*, *CCCF*, *CFCF*, *CSCF*, and *SFSF* edge conditions corresponding to nonhomogeneity m.

	m	$\alpha = 0.4$											
		$\beta_1 = \beta_2 = 0.0$		$\beta_1 = \beta_2 = 0.2$		$\beta_1 = \beta_2 = 0.4$		$\beta_1 = \beta_2 = 0.6$		$\beta_1 = \beta_2 = 0.8$		$\beta_1 = \beta_2 = 1.0$	
		K_1	K_2	K_1	K_2	K_1	K_2	K_1	K_2	K_1	K_2	K_1	K_2
CCCC	0.0	0.16035	0.61629	0.14653	0.56401	0.13369	0.51682	0.12193	0.47460	0.11124	0.43693	0.10159	0.40338
	0.2	0.16309	0.62562	0.14909	0.57262	0.13608	0.52474	0.12415	0.48192	0.11330	0.44372	0.10351	0.40966
	0.4	0.16578	0.63479	0.15160	0.58107	0.13843	0.53256	0.12632	0.48912	0.11533	0.45041	0.10539	0.41589
	0.6	0.16842	0.64384	0.15408	0.58943	0.14072	0.54026	0.12847	0.49622	0.11732	0.45701	0.10724	0.42198
	0.8	0.17102	0.65276	0.15651	0.59766	0.14299	0.54783	0.13057	0.50325	0.11927	0.46348	0.10906	0.42801
CCCF	0.0	0.18087	0.58993	0.16124	0.53036	0.14389	0.47897	0.12868	0.43448	0.11539	0.39575	0.10381	0.36182
	0.2	0.18375	0.59876	0.16385	0.53834	0.14625	0.48629	0.13082	0.44114	0.11735	0.40181	0.10559	0.10559
	0.4	0.18659	0.60749	0.16642	0.54623	0.14859	0.49342	0.13293	0.44768	0.11927	0.40781	0.10734	0.37288
	0.6	0.18938	0.61607	0.16896	0.55402	0.15088	0.50049	0.13501	0.45412	0.12115	0.41372	0.10906	0.37831
	0.8	0.19213	0.62452	0.17145	0.56166	0.15313	0.50743	0.13706	0.46046	0.12301	0.41956	0.11075	0.38368
CFCF	0.0	0.35632	0.77579	0.32644	0.68336	0.29794	0.60231	0.27100	0.53278	0.24575	0.47391	0.22229	0.42424
	0.2	0.36163	0.78754	0.33134	0.69379	0.30249	0.61164	0.27519	0.54111	0.24959	0.48129	0.22581	0.43090
	0.4	0.36684	0.79916	0.33618	0.70416	0.30695	0.62075	0.27930	0.54925	0.25338	0.48858	0.22927	0.43744
	0.6	0.37200	0.81060	0.34093	0.71427	0.31136	0.62977	0.28336	0.55726	0.25710	0.49574	0.23269	0.44385
	0.8	0.37705	0.82184	0.34564	0.72433	0.31570	0.63869	0.28736	0.56517	0.26077	0.50281	0.23605	0.45022
CSCF	0.0	0.36524	0.75543	0.33204	0.63718	0.30056	0.54029	0.27104	0.46229	0.24352	0.39993	0.21809	0.35010
	0.2	0.37061	0.76699	0.33697	0.64698	0.30508	0.54871	0.27515	0.46948	0.24726	0.40621	0.22149	0.35560
	0.4	0.37589	0.77830	0.34181	0.65666	0.30954	0.55697	0.27922	0.47661	0.25096	0.41237	0.22484	0.36103
	0.6	0.38114	0.78948	0.34661	0.66614	0.31393	0.56508	0.28322	0.48362	0.25461	0.41846	0.22815	0.36634
	0.8	0.38629	0.80054	0.35133	0.67557	0.31824	0.57312	0.28717	0.49053	0.25820	0.42446	0.23140	0.37162
SFSF	0.0	0.28765	1.6025	0.25987	1.4583	0.23487	1.3223	0.21258	1.1961	0.19281	1.0805	0.17531	0.97559
	0.2	0.29229	1.6282	0.26415	1.4821	0.23879	1.3442	0.21619	1.2162	0.19612	1.0989	0.17836	0.99243
	0.4	0.29688	1.6536	0.26835	1.5055	0.24265	1.3658	0.21973	1.2360	0.19938	1.1170	0.18136	1.0090
	0.6	0.30138	1.6786	0.27250	1.5286	0.24646	1.3871	0.22322	1.2554	0.20258	1.1347	0.18431	1.0252
	0.8	0.30581	1.7032	0.27656	1.5514	0.25020	1.4079	0.22665	1.2746	0.20574	1.1523	0.18721	1.0413

Table 4: Comparison of modes of frequency of the present study (orthotropic parallelogram plate) and obtained in [14] corresponding to tapering parameter β_1 for a fixed value of aspect ratio $a/b = 1.5$.

BC	β_1	$\alpha = \beta_2 = m = 0.0, \theta = 30^\circ$		$\alpha = \beta_2 = m = 0.4, \theta = 45^\circ$		$\alpha = \beta_2 = m = 0.8, \theta = 60^\circ$	
		λ_1	λ_2	λ_1	λ_2	λ_1	λ_2
SSSS	0.0	06.71	42.63	05.74	36.23	04.81	30.75
		11.18	**101.84**	**11.03**	**101.40**	**09.83**	**88.88**
	0.2	06.96	45.46	06.02	38.95	05.11	33.26
		12.33	**113.01**	**12.38**	**114.77**	**11.29**	**103.40**
	0.4	07.22	48.66	06.30	41.99	05.41	36.00
		13.52	**125.78**	**13.78**	**129.71**	**12.77**	**119.22**
	0.6	07.50	52.17	06.59	45.28	05.72	38.95
		14.73	**139.73**	**15.20**	**145.76**	**14.28**	**135.97**
	0.8	07.78	55.95	06.90	48.80	06.04	42.08
		15.98	**154.53**	**16.64**	**162.61**	**15.79**	**153.39**

Bold values are obtained from [14].

Table 5: Comparison of modes of frequency of the present study (orthotropic parallelogram plate) and obtained in [14] corresponding to tapering parameter β_2 for a fixed value of aspect ratio $a/b = 1.5$.

BC	β_2	$\alpha = \beta_1 = m = 0.0, \theta = 30^\circ$		$\alpha = \beta_1 = m = 0.4, \theta = 45^\circ$		$\alpha = \beta_1 = m = 0.8, \theta = 60^\circ$	
		λ_1	λ_2	λ_1	λ_2	λ_1	λ_2
SSSS	0.0	06.71	42.63	05.74	38.89	04.79	34.79
		11.18	**101.84**	**11.06**	**107.11**	**09.95**	**106.48**
	0.2	06.96	44.05	06.01	40.38	05.10	36.44
		12.32	**112.17**	**12.41**	**118.28**	**11.38**	**117.87**
	0.4	07.22	45.56	06.30	41.99	05.41	38.21
		13.51	**122.74**	**13.78**	**129.71**	**12.84**	**129.53**
	0.6	07.50	47.17	06.60	43.69	05.72	40.09
		14.73	**133.49**	**15.18**	**141.33**	**14.31**	**141.39**
	0.8	07.79	48.86	06.90	45.48	06.04	42.08
		15.97	**144.39**	**16.62**	**153.11**	**15.80**	**153.40**

Bold values are obtained from [14].

Table 6: Comparison of modes of frequency of the present study (orthotropic parallelogram plate) and obtained in [14] corresponding to nonhomogeneity m for a fixed value of aspect ratio $a/b = 1.5$.

BC	m	$\alpha = \beta_1 = \beta_2 = 0.0, \theta = 30^\circ$		$\alpha = \beta_1 = \beta_2 = 0.4, \theta = 45^\circ$		$\alpha = \beta_1 = \beta_2 = 0.8, \theta = 60^\circ$	
		λ_1	λ_2	λ_1	λ_2	λ_1	λ_2
SSSS	0.0	06.71	42.63	06.50	43.62	06.43	45.45
		11.18	**101.84**	**12.29**	**115.39**	**12.08**	**115.82**
	0.2	06.61	41.85	06.40	42.78	06.33	44.53
		11.78	**107.35**	**12.97**	**121.93**	**12.76**	**122.59**
	0.4	06.51	41.12	06.30	41.99	06.23	43.66
		12.50	**113.86**	**13.78**	**129.71**	**13.57**	**130.72**
	0.6	06.41	40.42	06.20	41.24	06.13	42.85
		13.36	**121.72**	**14.76**	**139.21**	**14.56**	**140.70**
	0.8	06.32	39.76	06.11	40.53	06.04	42.08
		14.43	**131.47**	**15.98**	**151.15**	**15.79**	**153.39**

Bold values are obtained from [14].

Table 7: Comparison of time period of the present study (orthotropic parallelogram plate) and obtained in [15] corresponding to tapering parameter β_1 for the fixed value of aspect ratio $a/b = 1.5$.

BC	β_1	$\theta = 0^{\circ}$		$\theta = 45^{\circ}$	
		K_1	K_2	K_1	K_2
CCCC	0.0	0.13285	0.51082	0.16123	0.61588
		0.03735	**0.14364**	**0.02407**	**0.09130**
	0.2	0.12599	0.48513	0.15323	0.58578
		0.03446	**0.13278**	**0.02229**	**0.08463**
	0.4	0.11912	0.45999	0.14520	0.55628
		0.03166	**0.12252**	**0.02229**	**0.07832**
	0.6	0.11240	0.43599	0.13733	0.52804
		0.02906	**0.11315**	**0.01896**	**0.07254**
	0.8	0.10595	0.41343	0.12974	0.50137
		0.02669	**0.10476**	**0.01749**	**0.06734**

Bold values are obtained from [15].

Table 8: Comparison of the time period of the orthotropic rectangle plate and obtained in [38] corresponding to nonhomogeneity m for a fixed value of aspect ratio $a/b = 1.5$.

BC	m	$\beta_1 = 0.0$		$\beta_1 = 0.4$	
		K_1	K_2	K_1	K_2
CCCC	0.0	0.13285	0.51082	0.11912	0.45999
		0.02978	**0.14981**	**0.02554**	**0.12964**
	0.2	0.13511	0.51855	0.12124	0.46709
		0.02980	**0.15016**	**0.02535**	**0.12919**
	0.4	0.13733	0.52619	0.12333	0.47407
		0.02982	**0.15045**	**0.02519**	**0.12883**
	0.6	0.13952	0.53370	0.12538	0.48092
		0.02983	**0.15070**	**0.02506**	**0.12853**
	0.8	0.14168	0.5411	0.12740	0.48770
		0.02984	**0.15091**	**0.02491**	**0.12827**

Bold values are obtained from [38].

Table 9: Comparison of the time period of the orthotropic rectangle plate and obtained in [38] corresponding to tapering parameter β_1 for aspect ratio $a/b = 1.5$.

BC	β_1	$m = 0.0$		$m = 0.4$	
		K_1	K_2	K_1	K_2
CCCC	0.0	0.13285	0.51082	0.13733	0.52619
		0.02978	**0.14981**	**0.02982**	**0.15045**
	0.2	0.12599	0.48513	0.13035	0.49983
		0.02755	**0.13908**	**0.02736**	**0.13886**
	0.4	0.11912	0.45999	0.12333	0.47407
		0.02554	**0.12964**	**0.02519**	**0.12883**
	0.6	0.11240	0.43599	0.11645	0.44941
		0.02374	**0.12132**	**0.02328**	**0.12009**
	0.8	0.10595	0.41343	0.10984	0.42625
		0.02214	**0.11396**	**0.02160**	**0.11243**

Bold values are obtained from [38].

Table 10: Comparison of modes of frequency of the isotropic square plate and obtained in [39–50] at *CCCC*, *SCSC*, *FCFC*, and *FSFS* edge conditions.

Boundary conditions	Ref	λ_1
CCCC	[39]	35.98
	[40]	35.99
	[41]	35.98
	[42]	35.98
	[43]	35.99
	[44]	35.99
	[45]	35.99
	[46]	35.99
	Present	**33.33**
SCSC	[39]	28.950
	[40]	28.951
	[47]	28.955
	[48]	29.951
	Present	**28.911**
FCFC	[39]	22.19
	[40]	22.27
	[49]	22.03
	Present	**22.43**
FSFS	[39]	9.631
	[40]	9.631
	[49]	9.631
	[50]	9.631
	Present	**10.574**

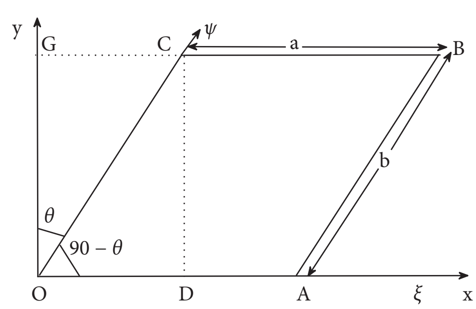

Figure 1: Orthotropic parallelogram plate with a skew angle θ.

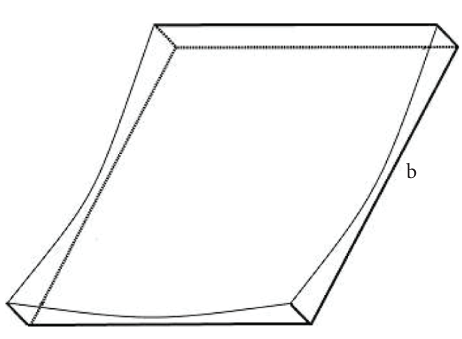

Figure 2: Orthotropic parallelogram plate having a two-dimensional circular thickness.

The flexural rigidities D_ζ, D_ψ and torsional rigidity $D_{\zeta\psi}$ of the plate are taken as in [14]

$$D_\zeta = \frac{E_\zeta l^3}{12\left(1 - \nu_\zeta \nu_\psi\right)}, D_\psi = \frac{E_\psi l^3}{12\left(1 - \nu_\zeta \nu_\psi\right)},$$
$$D_{\zeta\psi} = \frac{G_{\zeta\psi} l^3}{12}, D_1 = \nu_\zeta D_\psi = \nu_\psi D_\zeta, \tag{5}$$

where ν_ζ and ν_ψ are Poisson's ratios.

Using (3) and (4) in (5), we get

$$D_\zeta = \frac{E_1 h_0^3}{12(1-\nu_\zeta \nu_\psi)}\left[\frac{\left\{1-\alpha\left(1-\frac{\zeta^2}{a^2}\right)\left(1-\frac{\psi^2}{b^2}\right)\right\}}{\left\{\left(1+\beta_1\left(1-\sqrt{1-\frac{\zeta^2}{a^2}}\right)\right)\left(1+\beta_2\left(1-\sqrt{1-\frac{\psi^2}{b^2}}\right)\right)\right\}^3}\right],$$

$$D_\psi = \frac{E_2 h_0^3}{12(1-\nu_\zeta \nu_\psi)}\left[\frac{\left\{1-\alpha\left(1-\frac{\zeta^2}{a^2}\right)\left(1-\frac{\psi^2}{b^2}\right)\right\}}{\left\{\left(1+\beta_1\left(1-\sqrt{1-\frac{\zeta^2}{a^2}}\right)\right)\left(1+\beta_2\left(1-\sqrt{1-\frac{\psi^2}{b^2}}\right)\right)\right\}^3}\right],$$

$$D_{\zeta\psi} = \frac{G_0 h_0^3}{12}\left[\frac{\left\{1-\alpha\left(1-\frac{\zeta^2}{a^2}\right)\left(1-\frac{\psi^2}{b^2}\right)\right\}}{\left\{\left(1+\beta_1\left(1-\sqrt{1-\frac{\zeta^2}{a^2}}\right)\right)\left(1+\beta_2\left(1-\sqrt{1-\frac{\psi^2}{b^2}}\right)\right)\right\}^3}\right], \tag{6}$$

$$D_1 = \frac{E_1 h_0^3 \nu_\psi}{12(1-\nu_\zeta \nu_\psi)}\left[\frac{\left\{1-\alpha\left(1-\frac{\zeta^2}{a^2}\right)\left(1-\frac{\psi^2}{b^2}\right)\right\}}{\left\{\left(1+\beta_1\left(1-\sqrt{1-\frac{\zeta^2}{a^2}}\right)\right)\left(1+\beta_2\left(1-\sqrt{1-\frac{\psi^2}{b^2}}\right)\right)\right\}^3}\right].$$

Now, introducing nondimensional variable as

$$E_1^* = \frac{E_1}{1-\nu_\zeta\nu_\psi}, E_2^* = \frac{E_2}{1-\nu_\zeta\nu_\psi}, E^* = \nu_\zeta E_2^* = \nu_\psi E_1^*, \tag{7}$$

and components of E_1^*, E_2^*, E^* and G_0 are E_1^*, $E_2^* \sec\theta, E^* \sec\theta$, and $G_0 \sec\theta$, respectively, in ζ and ψ directions.

The equation for kinetic energy T_s and strain energy V_s for natural transverse vibration of a nonuniform orthotropic parallelogram is taken as in [15]

$$T_s = \frac{1}{2}\omega^2 \int_0^a \int_0^b \rho l \Phi^2 \cos\theta d\zeta d\psi, \tag{8}$$

$$\begin{aligned} V_s = \frac{1}{2}\int_0^a\int_0^b \Bigg[& D_\zeta \left(\frac{\partial^2\Phi}{\partial\zeta^2}\right)^2 + D_\psi\left(\frac{\partial^2\Phi}{\partial\zeta^2}\tan^2\theta - 2\frac{\partial^2\Phi}{\partial\zeta\,\partial\psi}\tan\theta\sec\theta + \frac{\partial^2\Phi}{\partial\psi^2}\sec^2\theta\right)^2 \\ & + 2D_1\left(\frac{\partial^2\Phi}{\partial\zeta^2}\right)\left(\frac{\partial^2\Phi}{\partial\zeta^2}\tan^2\theta + 2\frac{\partial^2\Phi}{\partial\zeta\,\partial\psi}\tan\theta\sec\theta + \frac{\partial^2\Phi}{\partial\psi^2}\sec^2\theta\right) + 4D_{\zeta\psi}\left(-\frac{\partial^2\Phi}{\partial\zeta^2}\tan\theta + \frac{\partial^2\Phi}{\partial\zeta\,\partial\psi}\sec\theta\right)^2\Bigg]\cos\theta\, d\zeta d\psi. \end{aligned} \tag{9}$$

The Rayleigh–Ritz method requires that maximum strain energy must be equal to maximum kinetic energy, i.e.,

$$J = \delta(V_s - T_s) = 0. \tag{10}$$

Substituting (8) and (9) in (10), we obtained

$$\begin{aligned} J = \frac{1}{2}\int_0^a\int_0^b \Bigg[& D_\zeta \left(\frac{\partial^2\Phi}{\partial\zeta^2}\right)^2 + D_\psi\left(\frac{\partial^2\Phi}{\partial\zeta^2}\tan^2\theta - 2\frac{\partial^2\Phi}{\partial\zeta\,\partial\psi}\tan\theta\sec\theta + \frac{\partial^2\Phi}{\partial\psi^2}\sec^2\theta\right)^2 \\ & + 2D_1\left(\frac{\partial^2\Phi}{\partial\zeta^2}\right)\left(\frac{\partial^2\Phi}{\partial\zeta^2}\tan^2\theta + 2\frac{\partial^2\Phi}{\partial\zeta\,\partial\psi}\tan\theta\sec\theta + \frac{\partial^2\Phi}{\partial\psi^2}\sec^2\theta\right) + 4D_{\zeta\psi}\left(-\frac{\partial^2\Phi}{\partial\zeta^2}\tan\theta + \frac{\partial^2\Phi}{\partial\zeta\,\partial\psi}\sec\theta\right)^2\Bigg]\cos\theta d\zeta d\psi \\ & - \frac{1}{2}\omega^2\int_0^a\int_0^b \rho l\Phi^2\cos\theta\, d\zeta\, d\psi. \end{aligned} \tag{11}$$

Using Eqs. (1), (6) and (7), (11) becomes

$$J = \int_0^a \int_0^b \left[\begin{array}{c} \left\{1 - \alpha\left(1 - \frac{\zeta^2}{a^2}\right)\left(1 - \frac{\psi^2}{b^2}\right)\right\}\{(1 + \beta_1\Upsilon_1)(1 + \beta_2\Upsilon_2)\}^3 \\ \left[\left\{\cos^4\theta + \frac{E_2^*}{E_1^*}\sin^4\theta + 2\frac{E^*}{E_1^*}\sin^2\theta\cos^2\theta + 4\frac{G_0}{E_1^*}\sin^2\theta\cos^2\theta\right\}\left(\frac{\partial^2\Phi}{\partial\zeta^2}\right)^2 + \frac{E_2^*}{E_1^*}\left(\frac{\partial^2\Phi}{\partial\psi^2}\right)^2\right. \\ +4\left\{\frac{E_2^*}{E_1^*}\sin^2\theta + \frac{G_0}{E_1^*}\cos^2\theta\right\}\left(\frac{\partial^2\Phi}{\partial\zeta\,\partial\psi}\right)^2 + 2\left\{\frac{E_2^*}{E_1^*}\sin^2\theta + \frac{E^*}{E_1^*}\cos^2\theta\right\}\left(\frac{\partial^2\Phi}{\partial\zeta^2}\right)\left(\frac{\partial^2\Phi}{\partial\psi^2}\right) \\ -4\left\{\frac{E_2^*}{E_1^*}\sin^3\theta + 2\frac{E^*}{E_1^*}\sin\theta\cos^2\theta + 2\frac{G_0}{E_1^*}\sin\theta\cos^2\theta\right\}\left(\frac{\partial^2\Phi}{\partial\zeta^2}\right)\left(\frac{\partial^2\Phi}{\partial\zeta\,\partial\psi}\right) \\ \left.-4\left\{\frac{E_2^*}{E_1^*}\sin\theta\right\}\left(\frac{\partial^2\Phi}{\partial\psi^2}\right)\left(\frac{\partial^2\Phi}{\partial\zeta\,\partial\psi}\right)\right]d\zeta\,d\psi \end{array} \right], \quad (12)$$

$$-\lambda^2\int_0^a\int_0^b[(1 - m\Upsilon_1)(1 + \beta_1\Upsilon_1)(1 + \beta_2\Upsilon_2)]\Phi^2 d\zeta\,d\psi,$$

where $\lambda^2 = 12\rho_0 a^2\cos^5\theta/E_1^* h_0^2$, $\Upsilon_1 = (1 - \sqrt{1 - \zeta^2/a^2})$, and $\Upsilon_2 = (1 - \sqrt{1 - \psi^2/b^2})$.

The two-term deflection function, which satisfies all the edge conditions, can be taken as in [6]

$$\Phi(\zeta,\psi) = \left[\left(\frac{\zeta}{a}\right)^e\left(\frac{\psi}{b}\right)^f\left(1 - \frac{\zeta}{a}\right)^g\left(1 - \frac{\psi}{b}\right)^h\right] \times \left[\sum_{i=0}^{N}\Omega_i\left\{\left(\frac{\zeta}{a}\right)\left(\frac{\psi}{b}\right)\left(1 - \frac{\zeta}{a}\right)\left(1 - \frac{\psi}{b}\right)\right\}^i\right], \quad (13)$$

which is the product of two functions. Here, the first function represents the boundary conditions depending on the value of e, f, g, and h, which can take different values depending upon the support edge condition. Values $0, 1, 2$ are assigned for free edge, simply supported, and clamped edge, respectively. The second function represents the number of modes of frequencies and $\Omega_i, i = 0, 1, 2, \ldots, N$, represents arbitrary constants.

In order to minimize the functional given in (12), we require the following condition:

$$\frac{\delta J}{\partial\Omega_i} = 0, i = 0, 1, 2, 3\ldots N. \quad (14)$$

After simplifying (14), we get a homogeneous system of equations in Ω_i whose nonzero solution gives an equation of frequency as

$$\left|P - \lambda^2 Q\right| = 0, \quad (15)$$

where $P = [p_{ij}]_{N+1}$ and $Q = [q_{ij}]_{N+1}$ are the square matrix of order $(n + 1), i = 0, 1, 2\ldots N$ and $j = 0, 1, 2\ldots N$.

The following expression is used for calculating the time period:

$$K = \frac{2\pi}{\lambda}, \quad (16)$$

where λ is a frequency obtained from (15).

3. Numerical Results and Discussion

For a fixed value of aspect ratio $a/b = 1.5$ and skew angle $\theta = 30^\circ$, the time period K for the first two modes of vibration of an orthotropic parallelogram plate with 2–D circular thickness and 1–D circular density under 2–D parabolic temperature is computed at *CCCC*, *CCCF*, *CFCF*, *CSCF* and *SFSF* edge conditions (refer Figure 3) corresponding to different plate parameters (tapering parameters β_1, β_2, thermal gradient α, and non-homogeneity m). In this study, the authors examined the impact of plate parameters on the behavior of time period of vibrational modes. During the calculation, the values of the following orthotropic material parameters are taken as in [15]:

$$\frac{E_2^*}{E_1^*} = 0.01, \frac{E^*}{E_1^*} = 0.3, \frac{G_0}{E_1^*} = 0.0333, \quad \frac{E_1^*}{\rho_0} = 3.0\times10^5 \text{ and } \nu_0 = 0.345. \quad (17)$$

All the results are conferred within Tables 1–3.

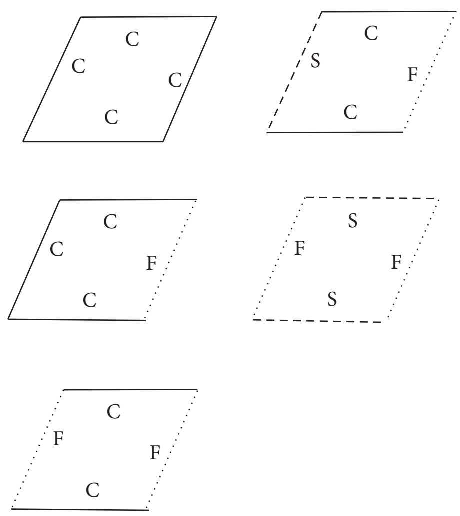

FIGURE 3: Orthotropic parallelogram plate with different edge conditions.

Table 1 represents the time period K of orthotropic parallelogram plate at *CCCC*, *CCCF*, *CFCF*, *CSCF*, and *SFSF* edge conditions for the fixed value of thermal gradient $\alpha = 0.4$ and nonhomogeneity $m = 0.2$ corresponding to both tapering parameters β_1 and β_2. The following observations can be drawn from Table 1:

(i) Time period K decreases corresponding to both increasing value of the tapering parameters β_1 and β_2 at all the edge conditions.

(ii) Under *CSCF* edge condition, the time periods K of vibrational modes are higher and less on *CCCC* edge condition. For different edge conditions, the time period K of vibrational modes in increasing order, corresponding to tapering parameters β_1 and β_2, is*CCCC* < *CCCF* < *SFSF* < *CFCF* < , *CSCF*.

(iii) The rate of decrement in the time period K corresponding to the tapering parameter β_1 is higher at *CCCC*, *CFCF*, and *SFSF* in comparison to the rate of decrement in the time period K corresponding to the tapering parameter β_2, while the rate of decrement corresponding to the tapering parameter β_2 is higher at *CCCF* and *CSCF* corresponding to tapering parameter β_2 in comparison to the rate of decrement in the time period K corresponding to the tapering parameter β_1.

(iv) For different edge conditions, the rate of decrement in time period K of vibrational modes in ascending order corresponding to tapering parameter β_1 is *CCCF* < CSCF < CFCF < CCCC < , *SFSF*, while for different edge conditions, the rate of decrement in time period K of vibrational modes in ascending order corresponding to tapering parameter β_2 is *SFSF* < *CCCC* < *CFCF* < *CSCF* < , *CCCF*.

Table 2 displays the time period K of the orthotropic parallelogram plate having variation in tapering parameters β_1 and β_2 from 0.0 to 0.8 and for fixed value of nonhomogeneity $m = 0.2$ corresponding to thermal gradient α at *CCCC*, *CCCF*, *CFCF*, *CSCF*, and *SFSF* edge conditions. The subsequent observations can be drawn from Table 2:

(i) As the value of thermal gradient α increases, the time period K of vibrational modes also increases but the time period K of vibrational modes decreases with the increasing value of tapering parameters β_1 and β_2 at all edge conditions.

(ii) Like in Table 1, the time period K of vibrational modes is higher on *CSCF* edge condition and less on *CCCC* edge condition. For different edge conditions, the time period K of vibrational modes in increasing order corresponding to thermal gradients α is *CCCC* < *CCCF* < *SFSF* < *CFCF* < *CSCF*.

(iii) At *CCCC* edge condition, the rate of increment in time period K is higher corresponding to thermal gradient α in comparison to the rate of decrement corresponding to tapering parameters β_1 and β_2, while on the rest of the edge conditions, i.e., *CCCF*, *CFCF*, *CSCF*, and *SFSF*, the rate of increment in time period K is smaller corresponding to thermal gradient α in comparison to the rate of decrement corresponding to tapering parameters β_1 and β_2.

(iv) The rate of increment in time period K of vibrational modes is higher on *CCCC* edge condition and less in *CCCF* edge condition corresponding to thermal gradient α, while the rate of decrement in time period K of vibrational modes is higher on *CCCF* edge condition and less in *CCCC* edge condition corresponding to tapering parameters β_1 and β_2. For different edge conditions, the rate of increment in time period K of vibrational modes in ascending order corresponding to thermal gradient α is *CCCF* < *CSCF* < *SFSF* < *CFCF* < , *CCCC*. But the rate of decrement in time period K of vibrational modes in ascending order corresponding to tapering parameters β_1 and β_2 is *CCCC* < *CFCF* < *SFSF* < *CSCF* < *CCCF*.

Table 3 provides the time period K of the orthotropic parallelogram plate at *CCCC*, *CCCF*, *CFCF*, *CSCF*, and *SFSF* edge conditions corresponding to nonhomogeneity m for a fixed value of thermal gradient $\alpha = 0.4$ and variable values of tapering parameters β_1 and β_2 from 0.0 to 0.8. From Table 3, the following facts can be interpreted:

(i) As the value of nonhomogeneity m increases, the time period K of vibrational modes also increases, but time period K of vibrational modes decreases with the increasing value of tapering parameters β_1 and β_2, β_1, β_2 at all edge conditions.

(ii) Like in Tables 1 and 2, here also the time period K of vibrational modes is higher on *CSCF* edge condition and less on *CCCC* edge condition. For different edge conditions, the time period K of vibrational modes in increasing order corresponding to nonhomogeneity m is *CCCC* < *CCCF* < *SFSF* < *CFCF* < , *CSCF*.

(iii) At all edge conditions, i.e., *CCCC*, *CCCF*, *CFCF*, *CSCF*, and *SFSF*, the rate of increment in time period K is less corresponding to nonhomogeneity m in comparison to the rate of decrement corresponding to tapering parameters β_1 and β_2.

(iv) The rate of increment in time period K of vibrational modes is higher on *CCCC* edge condition and less in *CSCF* edge condition corresponding to nonhomogeneity m, while the rate of decrement in time period K of vibrational modes is higher on *CCCF* edge condition and less in *CCCC* edge condition corresponding to tapering parameters β_1 and β_1, β_2. For different edge conditions, the rate of increment in time period K of vibrational modes in ascending order corresponding to nonhomogeneity m is *CSCF* < *CFCF* < *CCCF* < *SFSF* < *CCCC*. But the rate of decrement in time period K of vibrational modes in ascending order corresponding to tapering parameters β_1 and β_1, β_2 is *CCCC* < *CFCF* < *SFSF* < *CSCF* < *CCCF*.

4. Convergence of Results

In this section, the authors report a convergence study on modes of frequency λ for the following:

(i) Orthotropic parallelogram plate (by taking $\theta = 30^\circ, a/b = 1.5$ in the present study) at *CCCC*, *CCCF*, and *SFSF* edge conditions (refer Table 11)

(ii) Orthotropic rectangle plate (by taking $\theta = 0^\circ, a/b = 1.5$ in the present study) at *CCCC*, *CCCF*, *CFCF*, and *SFSF* edge conditions (refer Table 12)

(iii) Orthotropic square plate (by taking $\theta = 0^\circ, a/b = 1.0$ in the present study) at *CCCC*, *CCCF*, *CFCF*, *SFSF*, and *CSCF* edge conditions (refer Table 13)

When the order of approximation increased for all values of plate parameters in the ranges specified, i.e.,$\beta_1 = \beta_2 = m = \alpha = 0, E_2^*/E_1^* = 0.01, E^*/E_1^* = 0.3, G_0/E_1^* = 0.0333$, and $\nu_0 = 0.345$. All the results are presented in tabular form.

From Tables 11 and 12, the authors conclude that the first two modes of frequency λ of the orthotropic parallelogram plate at *CCCC*, *CCCF*, and *SFSF* edge conditions and orthotropic rectangle plate at *CCCC*, *CCCF*, *CFCF*, and *SFSF* edge conditions converge up to four decimal places in the fifth approximation, while Table 13 shows that the first two modes of frequency λ of orthotropic square plate at *CCCC*, *CCCF*, *CFCF*, *SFSF*, and *CSCF* edge conditions converge up to four decimal places in the sixth approximation.

5. Result Comparison

A comparative analysis of modes of frequency λ and time period K obtained in the present study was done with the following available published results:

(i) Modes of frequency λ of the orthotropic parallelogram plate obtained in [14] at *SSSS* edge condition corresponding to tapering parameters β_1 and β_2 and nonhomogeneity m (refer Tables 4–6)

(ii) Time period K of the orthotropic parallelogram plate obtained in [15] at *CCCC* edge condition corresponding to tapering parameter β_1 (refer Table 7)

(iii) Time period K of the orthotropic rectangular plate obtained in [38] at *CCCC* edge condition corresponding to nonhomogeneity m and tapering parameter β_1 (refer Tables 8 and 9)

(iv) Modes of frequency λ of isotropic square plate obtained in [39–50] at *CCCC*, *SCSC*, *FCFC*, and *FSFS* edge conditions (refer Table 10)

Tables 4 and 5 present the comparison of modes of frequency λ obtained in the present study (orthotropic parallelogram plate) and obtained in [14] corresponding to tapering parameters β_1 and β_2, respectively, for a fixed value of aspect ratio $a/b = 1.5$ and for the varying values of tapering parameters β_2 and β_1, nonhomogeneity m, thermal gradient α, and skew angle θ, i.e., $\beta_2 = m = \alpha = 0.0, 0.4, 0.8, \theta = 30^\circ, 45^\circ, 60^\circ$ (refer Table 4) and $\beta_1 = m = \alpha = 0.0, 0.4, 0.8, \theta = 30^\circ, 45^\circ, 60^\circ$ (refer Table 5) at *SSSS* edge condition. From Tables 4 and 5, the authors conclude that modes of frequency λ obtained in the present study (orthotropic parallelogram plate) is less in comparison to modes of frequency λ obtained in [14] with the increasing value of the tapering parameters β_1 as well as β_2 at *SSSS* edge condition.

The comparison of modes of frequency λ obtained in the present study (orthotropic parallelogram plate) and obtained in [14] corresponding to nonhomogeneity m for a fixed value of aspect ratio $a/b = 1.5$ and for the varying values of tapering parameters β_1 and β_2, thermal gradient α, and skew angle θ, i.e., $\beta_1 = \beta_2 = \alpha = 0.0, 0.4, 0.8, \theta = 30^\circ, 45^\circ, 60^\circ$ at *SSSS* edge condition, are displayed in Table 6. From Table 6, one can conclude that modes of frequency λ obtained in the present study (orthotropic parallelogram plate) is less in comparison to modes of frequency λ obtained in [14] with the increasing value of nonhomogeneity m at *SSSS* edge condition.

Table 7 shows the comparison of the time period K of the present study (orthotropic parallelogram plate) and obtained in [15] corresponding to tapering parameter β_1 for two different sets of values of skew angle θ, i.e., $\theta = 0^\circ, 45^\circ$, at *CCCC* edge condition for a fixed value of aspect ratio $a/b = 1.5$. Here, the authors exclude nonhomogeneity m, thermal gradient α, and tapering parameter β_2 because these plate parameters are not considered in [15]. Table 7 enlightens the fact that the time period K obtained in the present study is higher in comparison to the time period obtained in [15] for increasing value of tapering parameter β_1. But the rate of decrement in the time period K obtained in the present study is less in comparison to the rate of decrement obtained in [15].

For comparison of time period K of the orthotropic rectangle plate (by considering skew angle $\theta = 0^\circ$ in the present study) and obtained in [38], the authors exclude thermal gradient α and tapering parameter β_2 because both plates parameters are not considered in [38] (refer Tables 8 and 9). Table 8 incorporates the comparison of time period K of the orthotropic rectangle plate and obtained in [38]

Table 11: Convergence study of modes of frequency of the orthotropic parallelogram plate at *CCCC*, *CCCF*, and *SFSF* edge conditions.

N	*CCCC*		*CCCF*		*SFSF*	
	λ_1	λ_2	λ_1	λ_2	λ_1	λ_2
2	11.3063	43.3389	11.4976	37.1324	04.8196	26.2159
3	11.3061	42.7072	11.4948	35.5899	04.6538	24.0062
4	11.3061	42.7061	11.4936	35.5099	04.4441	23.9076
5	11.3061	42.7061	11.4936	35.5099	04.2815	23.7995

Table 12: Convergence study of modes of frequency of orthotropic rectangle plate at *CCCC*, *CCCF*, *CFCF*, and *SFSF* edge conditions.

N	*CCCC*		*CCCF*		*CFCF*		*SFSF*	
	λ_1	λ_2	λ_1	λ_2	λ_1	λ_2	λ_1	λ_2
2	12.2999	47.2968	12.5143	39.6281	09.8217	21.2732	04.8196	26.2159
3	12.2997	46.5478	12.5123	38.4012	08.1298	19.6771	04.6538	24.0062
4	12.2997	46.5454	12.5111	38.3289	04.7723	18.7564	04.4441	23.9076
5	12.2997	46.5454	12.5111	38.3289	04.7723	18.7564	04.4441	23.9076

Table 13: Convergence study of modes of frequency of the orthotropic square plate under *CCCC*, *CCCF*, *CFCF*, *SFSF*, and *CSCF* edge conditions.

N	*CCCC*		*CCCF*		*CFCF*		*SFSF*		*CSCF*	
	λ_1	λ_2	λ_1	λ_2	λ_1	λ_2	λ_1	λ_2	λ_1	λ_2
2	24.7880	98.0261	25.0290	75.9606	22.4259	44.6728	10.4990	56.9703	22.4249	41.5100
3	24.7880	95.3261	25.0287	75.1361	21.4911	41.3478	10.4247	49.7920	20.3751	38.6953
4	24.7880	95.3069	25.0282	75.1128	18.3431	38.1168	10.3099	49.7645	14.7061	36.6312
5	24.7880	95.1864	25.0279	75.0792	14.0662	36.4318	10.1751	49.7153	8.4351	35.7986
6	24.7880	95.1864	25.0279	75.0792	14.0662	36.4318	10.1751	49.7153	8.4351	35.7986

corresponding to nonhomogeneity m for two different sets of values of tapering parameter β_1, i.e., $\beta_1 = 0.0, 0.4$, at *CCCC* edge condition for a fixed value of aspect ratio $a/b = 1.5$. In Table 8, it has been seen that time period K as well as the rate of increment in time period K obtained in orthotropic rectangle plate is higher as compared to time period K as well as the rate of increment in time period K obtained in [38] with the increase in value of nonhomogeneity m.

Comparison of time period K of the orthotropic rectangle plate and obtained in [38] corresponding to tapering parameter β_1 for two different set of values of nonhomogeneity m, i.e., $m = 0.0, 0.4$, at *CCCC* edge condition for fixed value of aspect ratio $a/b = 1.5$ is incorporated in Table 9. Here, the authors observed that the behavior of time period K obtained for the orthotropic rectangle plate (refer Table 9) is the same as the behavior of the time period obtained for the orthotropic parallelogram plate (refer Table 7), i.e., the time period K obtained in the present study is higher in comparison to the time period obtained in [38] for increasing value of tapering parameter β_1. But the rate of decrement in the time period K obtained in the present study is less in comparison to the rate of decrement obtained in [38].

For comparison of the mode of frequency λ of an isotropic square plate (by considering skew angle $\theta = 0^\circ$ and aspect ratio $a/b = 1$ in the present study) with the mode of frequency λ obtained in [39–50], the authors take the value of the plate parameters as $E_2^*/E_1^* = 1, \alpha = \beta_1 = \beta_2 = m = 0.0$ (refer Table 10).

Table 10 incorporates the comparison of the mode of frequency λ (first mode) obtained for the square plate and obtained in [39–50] at *CCCC*, *SCSC*, *FCFC*, and *FSFS* edge conditions. From Table 10, the following facts can be drawn:

(i) The mode of frequency λ (first mode) obtained for the square plate is less in comparison to the mode of frequency λ (first mode) obtained in [39–46] at *CCCC* and [39, 40, 47, 48] *SCSC* edge condition, respectively.

(ii) The mode of frequency λ (first mode) obtained for the square plate is slightly higher in comparison to the mode of frequency λ (first mode) obtained in [39, 40, 49] at *FCFC* and [39, 40, 49, 50] *FSFS* edge condition, respectively.

6. Conclusions

The present study shows the effect of 2–D tapering parameters β_1, β_2, 2–D thermal gradient α, and 1–D nonhomogeneity m on the time period K of the mode of vibration of an orthotropic parallelogram plate at *CCCC*, *CCCF*, *CFCF*, *CSCF*, and *SFSF* edge conditions. From the above discussion and results comparison, the authors would like to conclude the following facts:

(i) In the case of two-dimensional circular variation in thickness, the modes of frequency λ obtained for orthotropic parallelogram plate (present study) are less in comparison to modes of frequency λ obtained in [14] in the case of two-dimensional linear variation in thickness (refer Tables 4 and 5) at *SSSS* edge condition.

(ii) In the case of one-dimensional circular variation in density, the modes of frequency λ obtained for orthotropic parallelogram plates (present study) are less in comparison to modes of frequency λ obtained in [14] in the case of one-dimensional linear variation in density (refer Table 6) at *SSSS* edge condition.

(iii) In the case of one-dimensional circular variation in thickness, the time period K obtained for the orthotropic parallelogram plate (present study) is higher in comparison to time period K obtained in [15] in the case of one-dimensional parabolic variation in thickness (refer Table 7) at *CCCC* edge condition.

(iv) In the case of one-dimensional circular variation in density, the time period K obtained for the orthotropic rectangle plate (present study) is higher in comparison to the time period K obtained in [38] in the case of one-dimensional linear variation in density (refer Table 8) at *CCCC* edge condition.

(v) In the case of one-dimensional circular variation in thickness, the time period K obtained for the orthotropic rectangle plate (present study) is higher in comparison to the time period K obtained in [38] in the case of one-dimensional parabolic variation in thickness (refer Table 9) at *CCCC* edge condition.

(vi) At *CCCC*, *CFCF*, and *SFSF* edge conditions, the tapering parameter β_1 dominates the rate of change in time period K more than the tapering parameter β_2, while at *CCCF* and *CFCF*, the tapering parameter β_2 dominates the rate of change in time period K more than the tapering parameter β_1 (refer Table 1).

(vii) At *CCCC* edge condition, the thermal gradient α dominates the rate of change in time period K more than the tapering parameters β_1, β_2, while at *CCCF*, *CFCF*, *CFCF*, and *SFSF*, the tapering parameters β_1, β_2 dominate the rate of change in time period K more than the thermal gradient α (refer Table 2).

(viii) At all edge conditions, i.e., *CCCC*, *CCCF*, *CFCF*, *CSCF*, and *SFSF*, the tapering parameters β_1, β_2 dominate the time period K (rate of decrement) more than the nonhomogeneity m (refer Table 3).

(ix) The time period K of modes of frequency decreases with the increasing value of tapering parameters β_1, β_2 (refer Table 1), while the time period K of modes of frequency increases with the increasing value of thermal gradient α and nonhomogeneity m (refer Tables 2 and 3).

From the abovementioned conclusions, we can say modes of frequency λ, time period K, and variation in time period K can be minimized and controlled by choosing the circular variation in the plate parameters.

Data Availability

The research data used to support the findings of this study are currently under embargo, while the research findings are commercialized. Requests for data, 6 months after the publication of this article, will be considered by the corresponding authors.

Conflicts of Interest

The authors declare that they have no conflicts of interest.

References

[1] S. Q. Li and H. Yuan, "A quasi-green function method for free vibration of clamped orthotropic parallelogram thin plates on winkler foundation," *Applied Mechanics and Materials*, vol. 397, pp. 431–434, 2013.
[2] A. K. Gupta, A. Kumar, and Y. K. Gupta, "Vibration of visco-elastic parallelogram plate with parabolic thickness variation," *Applied Mathematics*, vol. 1, no. 02, pp. 128–136, 2010.
[3] A. Gupta, A. Kumar, and D. Gupta, "Vibration of visco-elastic orthotropic parallelogram plate with linearly thickness variation," in *Proceedings of the International Conference in World Congress on Engineering and Computer Science 2007*, pp. 800–803, London, UK, July 2007.
[4] A. Sharma, "Natural vibration of parallelogram plate with circular variation in density," *Acta Technica*, vol. 63, no. 6, pp. 763–774, 2018.
[5] S. K. Sharma and A. K. Sharma, "Mathematically study on vibration of visco-elastic parallelogram plate," *Mathematical Models in Engineering*, vol. 1, no. 1, pp. 12–19, 2015.
[6] R. Bhardwaj, N. Mani, and A. Sharma, "Time period of transverse vibration of skew plate with parabolic temperature variation," *Journal of Vibration and Control*, vol. 27, no. 3-4, pp. 323–331, 2021.
[7] A. Khanna and P. Arora, "Effect of sinusoidal thickness variation on vibrations of non-homogeneous parallelogram plate with bi-linearly temperature variations," *Indian Journal of Science and Technology*, vol. 6, no. 9, pp. 1–7, 2013.
[8] A. Sharma, "Vibrational frequencies of parallelogram plate with circular variations in thickness," in *Soft Computing: Theories and Applications*, pp. 317–326, Springer, Berlin, Germany, 2018.
[9] A. M. Farag and A. S. Ashour, "Free vibration of orthotropic skew plates," *Journal of Vibration and Acoustics*, vol. 122, no. 3, pp. 313–317, 2000.
[10] C. V. Srinivasa, Y. J. Suresh, and W. P. Prema Kumar, "Experimental and finite element studies on free vibration of skew plates," *International Journal of Advanced Structural Engineering (IJASE)*, vol. 6, no. 1, pp. 1–11, 2014.
[11] A. K. Rai and S. S. Gupta, "Nonlinear vibrations of a polar-orthotropic thin circular plate subjected to circularly moving point load," *Composite Structures*, vol. 256, Article ID 112953, 2021.
[12] A. Sharma and N. Lather, "Natural vibration of skew plate on different set of boundary conditions with temperature gradient," *Vibroengineering Procedia*, vol. 22, pp. 74–80, 2019.

[13] A. Sharma, R. Bhardwaj, N. Lather, S. Ghosh, N. Mani, and K. Kumar, "Time period of thermal-induced vibration of skew plate with two-dimensional circular thickness," *Mathematical Problems in Engineering*, vol. 202212 pages, Article ID 8368194, 2022.

[14] A. K. Sharma, M. K. Dhiman, H. Singh, P. Prashar, and P. Sharma, "Effect of non-homogeneity with thickness and temperature variation on vibration of orthotropic parallelogram plate with simply supported edges," *ARPN Journal of Engineering and Applied Sciences*, vol. 14, no. 15, pp. 2757–2762, 2019.

[15] A. K. Gupta, A. Kumar, and D. V. Gupta, "Vibration of visco-elastic orthotropic parallelogram plate with parabolically thickness variation," *Annals of the Faculty of Engineering Hunedoara*, vol. 10, no. 2, pp. 61–70, 2012.

[16] V. Tahouneh, "Using an equivalent continuum model for 3d dynamic analysis of nanocomposite plates," *Steel and Composite Structures*, vol. 20, no. 3, pp. 623–649, 2016.

[17] V. Tahouneh, "Using modified halpin-tsai approach for vibrational analysis of thick functionally graded multi-walled carbon nanotube plates, Steel and Composite Structures," *International Journal*, vol. 23, no. 6, pp. 657–668, 2017.

[18] V. Tahouneh, "The effect of carbon nanotubes agglomeration on vibrational response of thick functionally graded sandwich plates, Steel and Composite Structures," *International Journal*, vol. 24, no. 6, pp. 711–726, 2017.

[19] V. Tahouneh, "Vibration and mode shape analysis of sandwich panel with mwcnts fg-reinforcement core, Steel and Composite Structures," *International Journal*, vol. 25, no. 3, pp. 347–360, 2017.

[20] V. Tahouneh, "Effects of cnts waviness and aspect ratio on vibrational response of fg-sector plate, Steel and Composite Structures," *International Journal*, vol. 25, no. 6, pp. 649–661, 2017.

[21] V. Tahouneh, "3-d vibration analysis of fg-mwcnts/phenolic sandwich sectorial plates, Steel and Composite Structures," *International Journal*, vol. 26, no. 5, pp. 649–662, 2018.

[22] V. Tahouneh, "Vibration and mode shape analysis of sandwich panel with mwcnts fg-reinforcement core, Steel and Composite Structures," *International Journal*, vol. 25, no. 3, pp. 347–360, 2017.

[23] V. Tahouneh, M. H. Naei, and M. M. Mashhadi, "Using iga and trimming approaches for vibrational analysis of l-shape graphene sheets via nonlocal elasticity theory, Steel and Composite Structures," *International Journal*, vol. 33, no. 5, pp. 717–727, 2019.

[24] V. Tahouneh, M. H. Naei, and M. M. Mashhadi, "Influence of vacancy defects on vibration analysis of graphene sheets applying isogeometric method: molecular and continuum approaches, Steel and Composite Structures," *International Journal*, vol. 34, no. 2, pp. 261–277, 2020.

[25] Y. Kiani, "Free vibration of fg-cnt reinforced composite skew plates," *Aerospace Science and Technology*, vol. 58, pp. 178–188, 2016.

[26] Y. Kiani, R. Dimitri, and F. Tornabene, "Free vibration of fg-cnt reinforced composite skew cylindrical shells using the Chebyshev-ritz formulation," *Composites Part B: Engineering*, vol. 147, pp. 169–177, 2018.

[27] Y. Kiani, "Thermal buckling of temperature-dependent fg-cnt-reinforced composite skew plates," *Journal of Thermal Stresses*, vol. 40, no. 11, pp. 1442–1460, 2017.

[28] Y. Kiani and M. Mirzaei, "Rectangular and skew shear buckling of fg-cnt reinforced composite skew plates using ritz method," *Aerospace Science and Technology*, vol. 77, pp. 388–398, 2018.

[29] Y. Kiani, "Nurbs-based thermal buckling analysis of graphene platelet reinforced composite laminated skew plates," *Journal of Thermal Stresses*, vol. 43, no. 1, pp. 90–108, 2020.

[30] Y. Kiani and K. K. Żur, "Free vibrations of graphene platelet reinforced composite skew plates resting on point supports," *Thin-Walled Structures*, vol. 176, Article ID 109363, 2022.

[31] S. Kumar and P. Jana, "Application of dynamic stiffness method for accurate free vibration analysis of sigmoid and exponential functionally graded rectangular plates," *International Journal of Mechanical Sciences*, vol. 163, Article ID 105105, 2019.

[32] L. Wang, J. Liu, C. Yang, and D. Wu, "A novel interval dynamic reliability computation approach for the risk evaluation of vibration active control systems based on pid controllers," *Applied Mathematical Modelling*, vol. 92, pp. 422–446, 2021.

[33] S. Kumar, V. Ranjan, and P. Jana, "Free vibration analysis of thin functionally graded rectangular plates using the dynamic stiffness method," *Composite Structures*, vol. 197, pp. 39–53, 2018.

[34] H. Liu and Z. Lyu, "Modeling of novel nanoscale mass sensor made of smart fg magneto-electro-elastic nanofilm integrated with graphene layers," *Thin-Walled Structures*, vol. 151, Article ID 106749, 2020.

[35] Ö. Civalek, "Geometrically nonlinear dynamic and static analysis of shallow spherical shell resting on two-parameters elastic foundations," *International Journal of Pressure Vessels and Piping*, vol. 113, pp. 1–9, 2014.

[36] Ö. Civalek and A. K. Baltacıoglu, "Free vibration analysis of laminated and fgm composite annular sector plates," *Composites Part B: Engineering*, vol. 157, pp. 182–194, 2019.

[37] H. Ersoy, K. Mercan, and Ö. Civalek, "Frequencies of fgm shells and annular plates by the methods of discrete singular convolution and differential quadrature methods," *Composite Structures*, vol. 183, pp. 7–20, 2018.

[38] A. Gupta, N. Agarwal, D. Gupta, S. Kumar, and P. Sharma, "Study of non-homogeneity on free vibration of orthotropic visco-elastic rectangular plate of parabolic varying thickness," *Advanced Studies of Theory Physics*, vol. 4, no. 10, pp. 467–486, 2010.

[39] Y. Kumar and R. Lal, "Vibrations of nonhomogeneous orthotropic rectangular plates with bilinear thickness variation resting on winkler foundation," *Meccanica*, vol. 47, no. 4, pp. 893–915, 2012.

[40] A. W. Leissa, "The free vibration of rectangular plates," *Journal of Sound and Vibration*, vol. 31, no. 3, pp. 257–293, 1973.

[41] S. Dickinson and E. Li, "On the use of simply supported plate functions in the Rayleigh-ritz method applied to the flexural vibration of rectangular plates," *Journal of Sound and Vibration*, vol. 80, no. 2, pp. 292–297, 1982.

[42] R. B. Bhat, "Natural frequencies of rectangular plates using characteristic orthogonal polynomials in Rayleigh-ritz method," *Journal of Sound and Vibration*, vol. 102, no. 4, pp. 493–499, 1985.

[43] A. Khanna and A. K. Sharma, "Natural vibration of visco-elastic plate of varying thickness with thermal effect," *Journal of Applied Science and Engineering*, vol. 16, no. 2, pp. 135–140, 2013.

[44] A. Sharma, "Vibration of nonhomogeneous square plate with circular variation in density," in *Engineering Vibration,*

Communication and Information Processing, pp. 253–263, Springer, Berlin, Germany, 2019.

[45] A. Khanna, R. Deep, and D. Kumar, "Effect of thermal gradient on vibration of non-homogeneous square plate with exponentially varying thickness," *Journal of Solid Mechanics*, vol. 7, no. 4, pp. 477–484, 2015.

[46] A. Sharma, N. Mani, R. Bhardwaj, and K. Kumar, "Thermal vibration of rectangle plate with two-dimensional circular thickness effect," *Mathematical Problems in Engineering*, vol. 20229 pages, Article ID 9744671, 2022.

[47] Y. Wang and Z.-m. Wang, "Transverse vibration of visco-elastic rectangular plate with linearly varying thickness and multiple cracks," *Journal of Sound and Vibration*, vol. 318, no. 4-5, pp. 1005–1023, 2008.

[48] H. Kobayashi and K. Sonoda, "Vibration and buckling of tapered rectangular plates with two opposite edges simply supported and the other two edges elastically restrained against rotation," *Journal of Sound and Vibration*, vol. 146, no. 2, pp. 323–337, 1991.

[49] T. Mizusawa, "Natural frequencies of rectangular plates with free edges," *Journal of Sound and Vibration*, vol. 105, no. 3, pp. 451–459, 1986.

[50] C. Bert and M. Malik, "Free vibration analysis of tapered rectangular plates by differential quadrature method: a semi-analytical approach," *Journal of Sound and Vibration*, vol. 190, no. 1, pp. 41–63, 1996.